RESEARCH PAPER

Effect of welding parameters on resistance thermocompression microwelded joint of insulated copper wire

Zhiyuan Cui[1] · Yuanbo Li[1,2] · Lingyu Chen[1] · Songjie Wen[1] · Songming Guo[1]

Abstract

Insulated copper wire has been widely used in many industries, but the insulating coating must be removed before welding because it will hinder the formation of joints. Therefore, in this work, the resistance thermocompression microwelding process for insulated wire without removing the coating in advance was proposed. Through detailed mechanical testing and metallurgical examination, the effects of welding voltage on the joint appearance, joint macro-/microstructure, joint breaking force, and joint fracture mode were investigated. The results showed that joints were achieved by solid-state bonding. As the welding voltage was further increased, the joint breaking force increased first and then decreased. Corresponding to the change of the welding voltage, the fracture mode of the joints changed from interfacial fracture to partial pullout fracture. The fracture position also moved backwards gradually, which was caused by the expansion of the bonding area, the improvement of the interfacial strength, and the amount of heat input. Finally, an orthogonal experiment was conducted to investigate the significance level of three parameters. Under the optimal for joint breaking force parameters (2.1 V, 24 ms, and 12 N), the average achievable force was 1.1723 N, which was about 83.7% of the breaking force of the as-received wire.

Keywords Insulated copper wire · Resistance thermocompression microwelding · Fracture mode · Solid-state bonding · Multi-factor orthogonal experiment

1 Introduction

Wire bonding technology is widely used in many applications such as IC packaging, coils used in electronic circuits, motors, and transformers integrated into various electrical devices and machines [1, 2]. Due to its mechanical and electrical properties, high reliability, and ease of assembly, gold (Au) wire has been used in this technology for more than 55 years. However, due to its increasing cost, alternative materials for wire bonding have been considered [3]. Copper (Cu) wire is the most

✉ Yuanbo Li
liyuanbo@gdut.edu.cn

1 Guangzhou Key Laboratory of Nontraditional Machining and Equipment, Guangdong University of Technology, Guangzhou 510006, People's Republic of China

2 State Key Laboratory of Precision Electronic Manufacturing Technology and Equipment, Guangdong University of Technology, Guangzhou 510006, People's Republic of China

preferred alternative material because Cu wire has lower electrical resistance, higher thermal conductivity, and lower cost than Au wire [4, 5].

Although Cu wire has many advantages over Au wire, there are still some problems to be solved in the application of Cu [6]. For instance, Cu wire is easy to be oxidized in air, and ultrasonic wire bonding requires the nitrogen atmosphere or other inert atmosphere to remove the thermal oxide layer [7]. In addition, higher electrode force or greater ultrasonic energy may damage the substrate because Cu wire is harder than Au wire [8]. Furthermore, higher wire sweeping and shorting rejects in fine copper wire bonding lead to higher process yield loss [9].

Insulated copper wire has a conductive core and electrically insulated coating. This coating can prevent wires shorting and allows longer wires, wires crossing, and wires touching, but it will block the conduction of welding current so that the joints cannot be formed. In addition, the residual carbides in the faying surface of the welded joint can interrupt the electrical current through the contact interface. The non-interruption conduction of electrical current across the contact interface can only be achieved through clean metal-to-metal contact.

Therefore, it is very important and valuable to develop a more reliable and cost-effective welding process for insulated copper wire, such as stitch bonding [10, 11], ultrasonic welding (UW) [12, 13], laser microwelding (LMW) [14, 15], friction stir welding (FSW) [16], parallel gap resistance welding (PGRW) [17, 18], and resistance microwelding (RMW) [19, 20].

A research on stitch bonding process with 20-μm insulated Cu wire on Au-plated Al substrate was presented in Ref [10], and compared the results with stitch bonds of bare Cu wire in details. The stitch pull strength of the insulate Cu stitch bond samples was 37% than that of bare Cu, and the strength required isothermal aging at 255°C for 78 h to meet the industry reliability standard. In addition, the residual insulated coating in the bonding interface may result in lower stitch pull strength.

A parallel gap resistance microwelding process for insulated Cu wire and Au plating was proposed, and a detailed investigation was performed from aspects of the orthogonal experiment, effect of welding parameters on microstructure of joints, and bonding mechanism [21]. The results showed that during the welding process, no weld nugget was formed, which indicated that the bonding mechanism for insulated wire/Au plating interconnection was solid-state bonding. It was found that welding voltage had the greatest effect on joint quality. At low heat input, the joints fractured at the interface. As the heat input was increased, the fracture mode changed to neck fracture. However, this process required advanced removal of coating, which could have a negative impact on its cost and efficiency.

The RMW of 100-μm insulated copper wire to phosphor bronze sheet has been experimentally studied, mainly focusing on the effect of process parameters on bonding performance. During a single welding cycle of the RMW, a special electrode configuration was employed to first eliminate the coating in the preheating stage, and then obtain the bonding joints in the welding stage. The electrode configuration included an upper electrode and a lower electrode to form a welding circuit. The upper electrode was composed of two separate chromium-copper alloy semi-cylinders with an embedded cylindrical tip (molybdenum), and the lower electrode was made of a copper-chromium alloy cylinder. The research indicated that during RMW, the formation of the joint can be divided into three stages, i.e. cold wire deformation, melting and displacement of the coating, and solid-state bonding. In this process, preheating current was used to remove the coating in advance; however, the long preheating time (120 ms) reduced the production efficiency of RMW. In addition, the RMW process required both sides accessible. However, in the production of many electronic products, only one-sided welding was allowed and the production space was relatively narrow, which limited the practical application of

RMW in small-size welding. Moreover, the electrode used in RMW can cause depression, resulting in weakness at the joint neck [22].

As mentioned above, some insulated Cu wire bonding technologies require advanced removal of the coating in advance (PGRW, UW, and FSW). Although there is no need to remove the coating in advance in some technologies, there are residual carbides in the faying surface, such as stitch bonding, or the working conditions are extremely strict, which is impractical in the manufacturing process (LMW and RMW). In this paper, the resistance thermocompression microwelding (RTMW) process with great economic and applicability was proposed, and the effect of voltage on the joint quality was investigated by detailed mechanical testing and metallurgical examination. Furthermore, combined with the results of the single-factor experiment, a multi-factor orthogonal experiment was conducted to determine the significance level of each affecting parameter for the joint quality and the optimal combination of process parameters for the joint breaking force. Finally, the bonding joints with better performance were obtained, and this process will soon be applied to the practical welding of insulated copper wires.

2 Materials and methods

In order to overcome the above shortcomings, make the process parameters easy to control, and ensure the high performance and high reliability of the welding joint, the RTMW process was applied to achieve the bonding between the fine insulated wire and thin sheet. The specific process is shown in Fig. 1. Different from the RMW process in Ref [22], the RTMW process used only one electrode with a narrow gap opening slot, which made the current form a loop inside the electrode, thereby generating Joule heat using the bulk resistance of the electrode. Finally, only in the welding stage, the combined effect of heat and electrode force was used to remove the coating and obtain the joint. The schematic diagram of the welding schedule for RTMW is shown in Fig. 2.

Class P155p round insulated copper wire (Elektrisola Co., Ltd., DE) and 0.2-mm-thick commercial phosphor bronze sheet (half-hard as-rolled) were used in this study. The Cu wire included bare wire with a diameter of 100-μm (Cu-ETP, annealed after cold-drawn) and 15-μm-thick modified polyurethane coating. The chemical composition of the phosphor bronze sheet is listed in Table 1. All the sheet specimens were machined into the dimensions of 18 × 7 mm. Furthermore, in order to ensure that the experiment had consistent welding conditions with actual production, all samples were not cleaned before welding.

As for micro-wire bonding equipment, a GW-CN-01 precision linear spot-welding machine was used, which could bond wires with a diameter of 40~300 μm. The welding

Fig. 1 (a) The RTMW equipment used for insulated copper wire bonding. (b) Schematic diagram of RTMW. (c) High-magnification image of the circled area in a
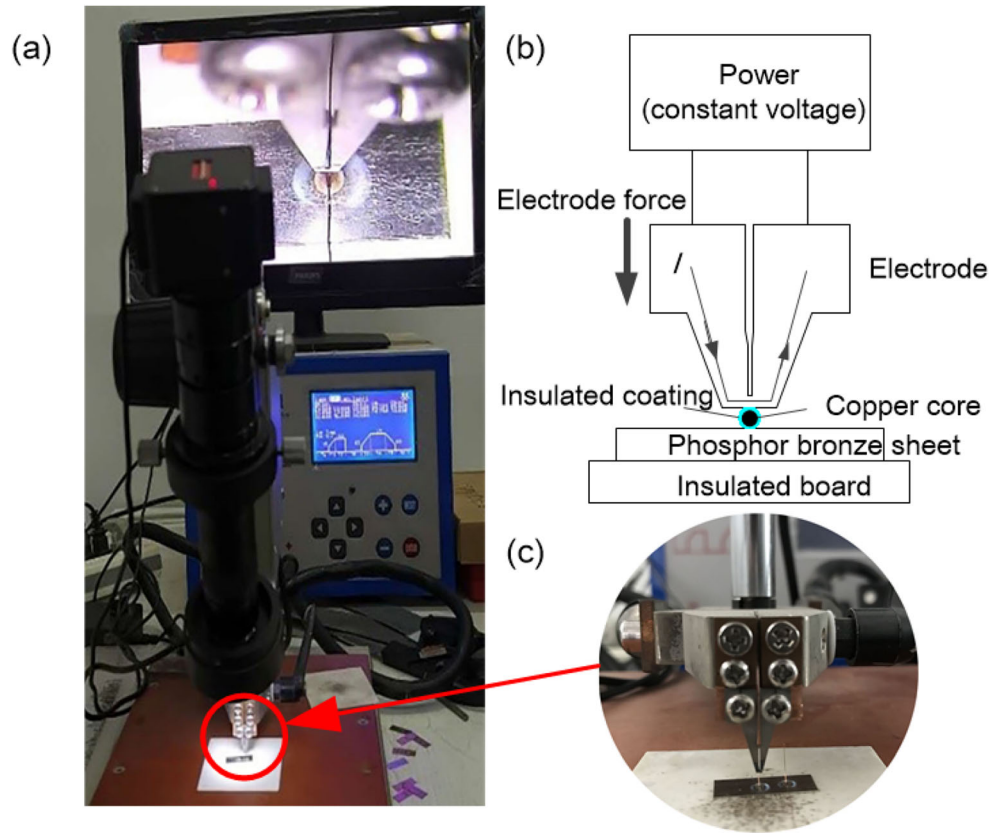
power was provided by a linear DC supply with the rated power of 220 V/50 Hz, the maximum output current of 1000 A, and the output pulse time of 2~50 ms. A 5°-bevel-ended, RWMA Class 14 (molybdenum) electrode (pedal control) was used for welding. The geometry and dimensions of the electrode are shown in Fig. 3(a). When the electrode force reached the pre-set value, the PLC received an electrical signal from the pressure sensor to trigger the discharge of the welding power supply, and finally, the joints were obtained by RTMW. It is worth mentioning that the electrode tip was machined into a 5° bevel. On the one hand, as shown in position 1 in Fig. 3(b), it will cause "Depression" at the front-end

of the joint after welding, which is beneficial to remove the extension of the wire. On the other hand, the electrode will not damage the wire at the rear-end of the joint (for example, the smooth "Transition" in position 2 in Fig. 3(c)), which can prevent stress concentration, because the wire at rear-end wire of the joint is used for electrical connection.

After welding, the joint breaking force, a foremost indicator of joint quality, was measured by tensile testing using a CMT8051 universal mechanical tester at a pulling speed of 10 mm/min; the tensile direction was vertical to the phosphor bronze sheet, as shown in Fig. 4. Furthermore, the length (L) and width (W) of joints, which were also important indicators to evaluate joint quality, were measured by a LEXT OLS4100 type confocal scanning laser microscope (OM). In each condition, five joints were tested, and the average breaking force, length, and width of the joints were obtained. Figure 5 illustrates the schematic diagram of metallographic specimens and the dimensions of the welded joints. By cutting the cross section perpendicular to a plane position on the surface, the metallographic specimens for the microstructure test were
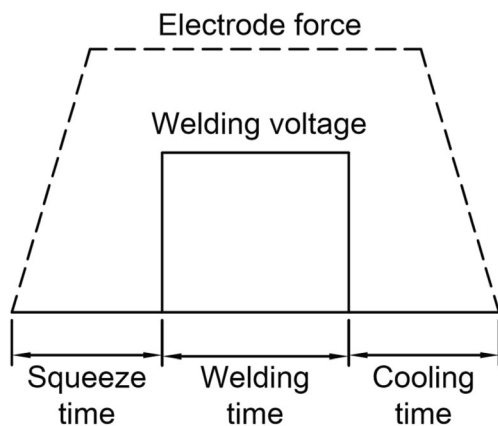
Fig. 2 Schematic diagram of welding schedule

Table 1   Chemical composition of phosphor bronze sheet (wt.%)

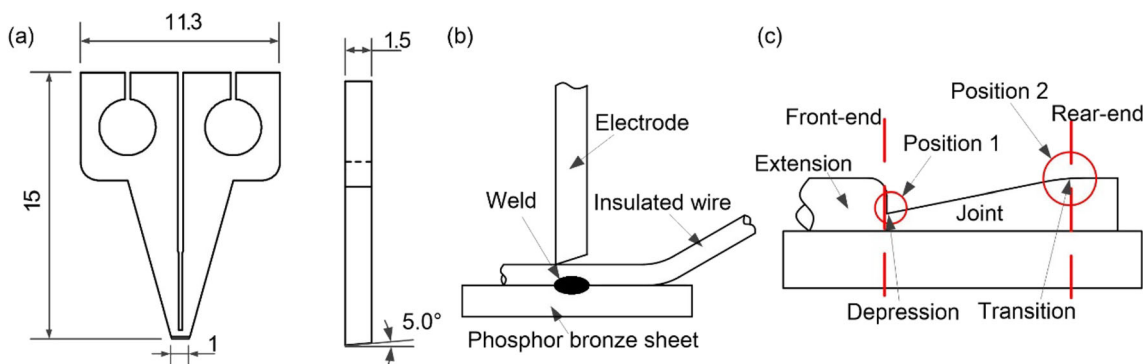| Sn	P	Fe	Pb	Cu
5.6	0.16	0.08	0.07	Bal.

Fig. 3 (**a**) Geometry and dimensions of the electrode (mm). (**b**) Welding process setup. (**c**) Shape of the welded joint

obtained. These positions were uniformly fixed at distance of 200 μm from the front-end of the joints. Then, the specimens' cross sections were ground, polished, and etched with a solution of 5 g $FeCl_3$, 20 ml HCl, and 120 ml H_2O for 3 to 5 s to reveal the microstructure of the joints. The appearance, microstructure, and compositions of the joints were examined by OM and a scanning electron microscope (SEM, Hitachi S-3400N) with energy-dispersive spectroscopy (EDS). Under a load of 25 g, the Vickers microhardness was also measured on the cross sections of the joints.

3 Results and discussion

3.1 Joint geometry and appearance

Figure 6 shows typical joints made at different welding voltages. The welding time was fixed at 20 ms and the electrode force was set to 12 N. In the squeezing stage, the insulated copper wire was first mechanically deformed, and dents appeared on the wire, but no mechanical fracture or displacement from the Cu wire of the insulation was observed. The upper surface of the

coating was immediately melted by the heat generated by the welding current flowing through the electrode, and the molten insulation rapidly shrank back because of the heat conduction along the wire. It was observed that there was ablation of insulation scatter around the joints (the dark rings in Fig. 6(a–e), and the wire to be bonded had both ends exposed. Unlike those observed in RMW of insulated wire [22], no liquefied insulation was trapped between the wire and the sheet outside the joint (Fig. 6(f)). As the welding voltage increased, less scattered insulation was observed on the sheet, which was due to the evaporation of insulation. When the welding voltage reached 2.15 V, melting occurred on the upper surface of the joint, obvious pits and protuberances appeared, and severe electrode sticking to the wire was observed (Fig. 6(e)).
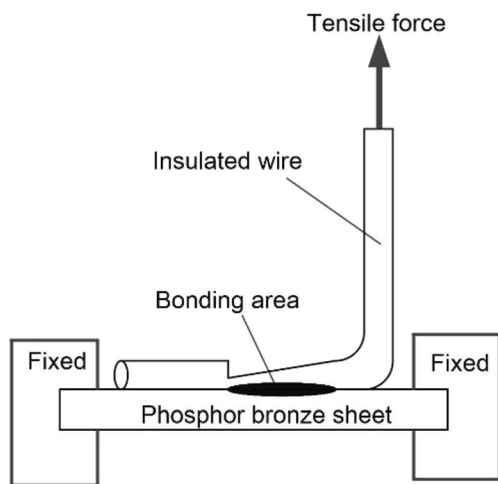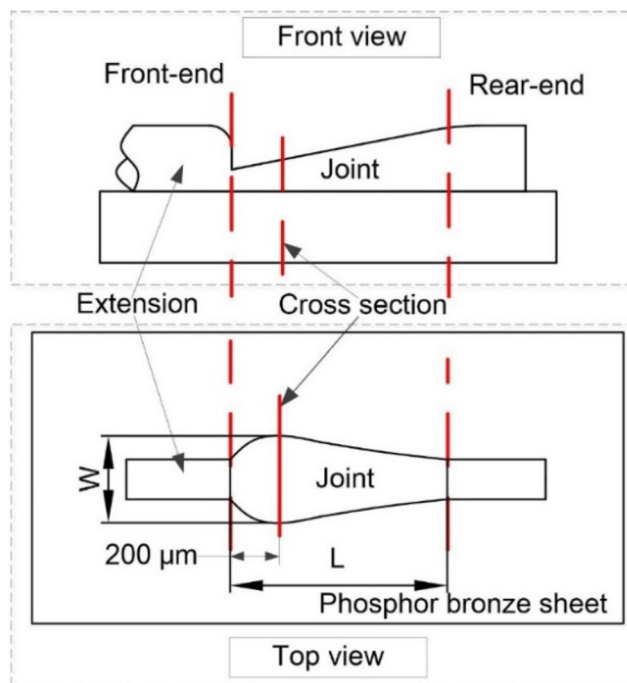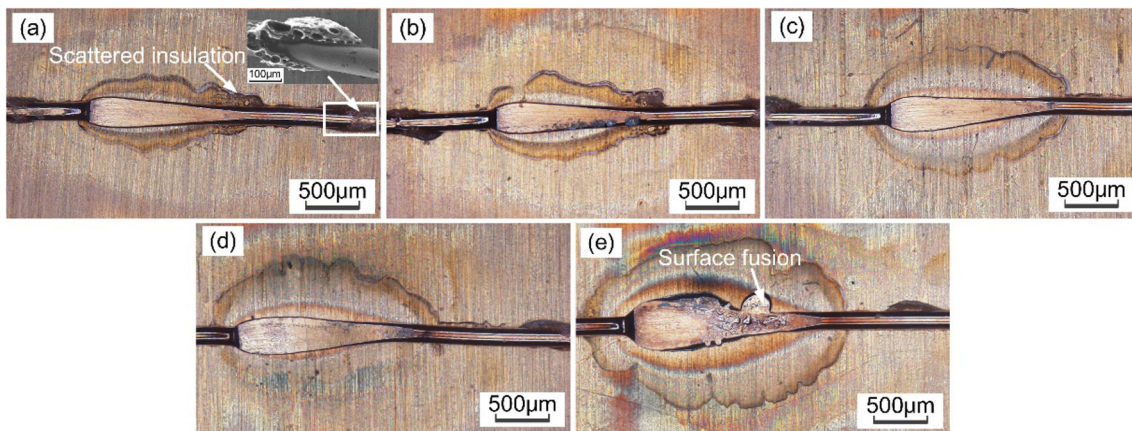

Fig. 4 Schematic diagram of tensile test

Fig. 5 Schematic diagram of metallographic samples and measurement of joints size, where L is the length of the joint and W is width of the joint

Fig. 6 Top view of the appearance of the joints at different welding voltages: (**a**) 1.75 V; (**b**) 1.85 V; (**c**) 1.95 V; (**d**) 2.05 V; (**e**) 2.15 V

## 3.2 Macro-/microstructure of the bonding interface

The cross sections of the typical joint at various welding voltages are shown in Fig. 7. It can be seen from Fig. 7 that under different voltages, the wire was deformed to a different extent. As the voltage increased, the width of the joint increased accordingly. As the welding voltage increased in the range of 1.75 to 2.05 V, there was no visible interfacial melting in the joints, and the bonding line was distinctly presented at the faying surfaces (Fig. 7(a–d)). Therefore, it can be speculated that the insulated wire was predominantly bonded to the sheet by a solid-state bonding process. When the welding voltage was 2.15 V, melting occurred on the upper surface of the phosphor bronze sheet, and the bonding line was no longer straight. Due to the action of

electrode force, most of the molten material formed at the interface were squeezed out of the interfacial area, forming a "fillet" and increasing the bonding area (Fig. 7(e)).

The microstructures at the edge and in the central region of these joints are shown in Fig. 8. At a lower voltage of 1.75 V, the insulated wire was only locally bonded to the sheet as shown by the dashed area in Fig. 8(a). Due to the surface roughness, the gap between the insulated wire and the sheet still existed. When the welding voltage was increased and exceeded 1.85 V, the gap completely disappeared, and the bond of two base metals became tighter. When the voltage reached 2.15 V, many voids were observed in the cross section of the insulated wire, and due to the reorientation of grains and the migration of grain boundaries, the bonding line was

Fig. 7 SEM images of microstructure of the cross section of the joints at different welding voltages: (**a**) 1.75V, (**b**) 1.85V, (**c**) 1.95V, (**d**) 2.05V, (**e**) 2.15V
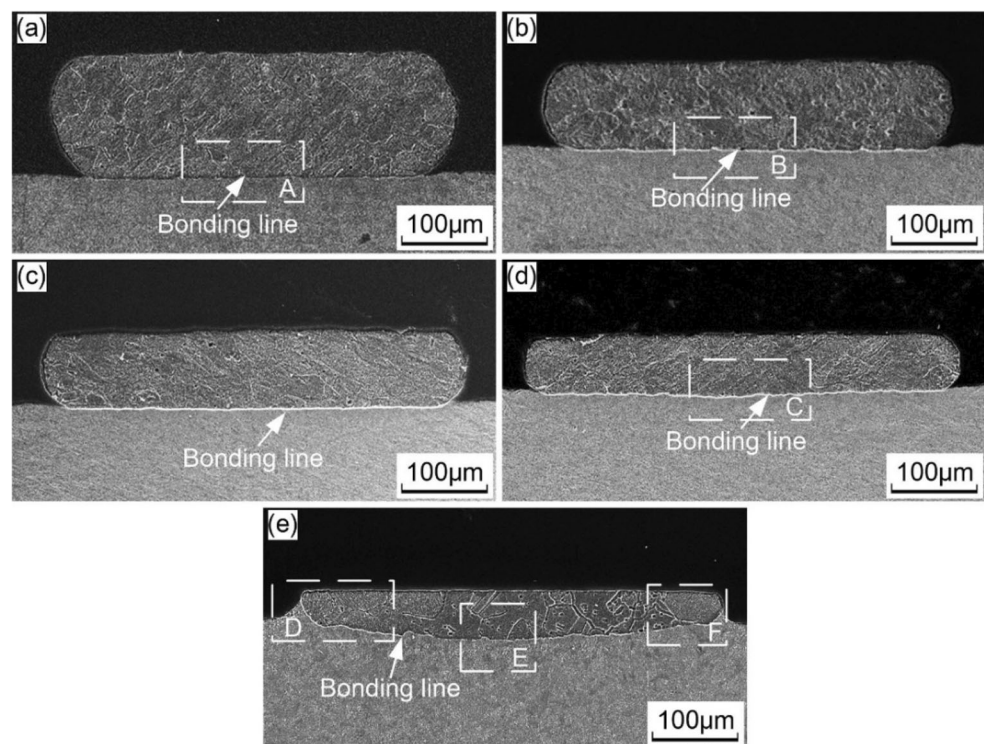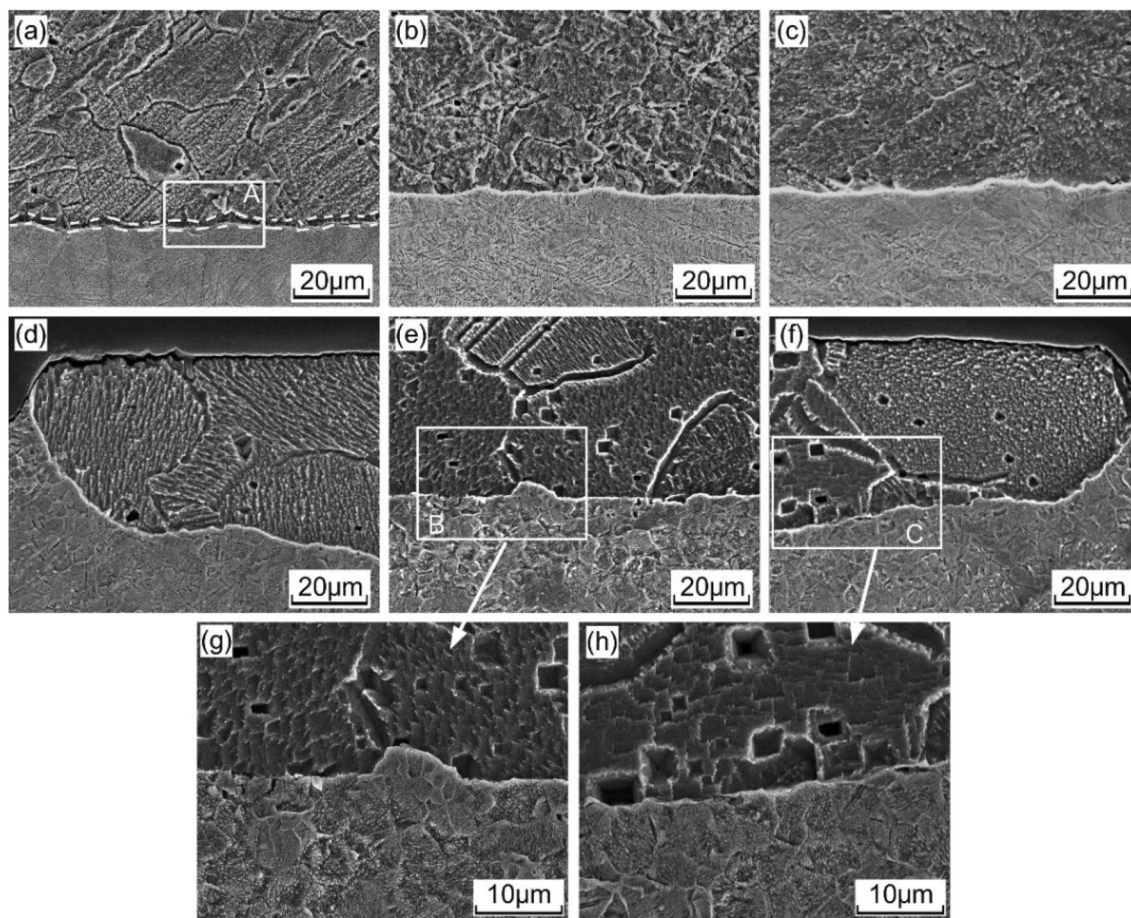
Fig. 8 (**a–f**) Microstructures correspond to areas A–F in Fig. 7, respectively. (**g, h**) The details of the inconspicuous bonding lines in area B and area C, respectively

still distinct but became thinner, as shown in Fig. 8(g) and (h). Moreover, as the voltage increased, the annealed microstructure of Cu wire became significantly coarsening. At the welding voltage of 2.15 V, the annealing twins were observed near the bonding interface (Fig. 8(d–f)). In addition, when the melting at the interface occurred, a dense interface was formed on the cross section of the joint, and no voids or defects adjacent to the interface were observed in the region where molten metal has been solidified. The results indicated that the molten material had good fluidity. In addition, no transient liquid phase or molten nugget was observed at the bond interface. It was worth noting that with the increase of welding heat, the microstructures of the phosphor bronze sheet near the faying surface hardly changed, while the microstructures of the sheet in RMW were coarsening. It was deduced that the difference was due to the difference between the objects that generated Joule heat in the RTMW process and the RMW process. The RTMW process conducted the Joule heat generated by bulk resistance of the electrode to the base metals, and then used the resistance heat and electrode force to achieve joint bonding, unlike the resistance heat generated at the faying surface in the RMW process.

EDX analysis was conducted to investigate the microstructure and composition of the bonding interface, and to verify whether the existence of residual carbide in the faying surface. Figure 9 shows the detailed SEM images of the central and edge regions of the joint at the welding voltage of 1.75V (Fig. 7(a)). The EDX analysis results of regions A, D, and F are listed in Table 2. The microstructure at the edge (regions D and E) and the centre (region A in Fig. 8) of the interface demonstrated that there were no residual carbide layers trapped in the faying surface, which was consistent with the results determined by the EDS analysis.

3.3 Joint breaking force and fracture mode

Figure 10 shows the effects of welding voltage on the joint braking force (as an indicator of joint strength) and width. From the result, as the voltage increased, the width increased monotonically, but the breaking force first increased and then decreased. As the welding voltage increased from 1.75 to 2.05 V, the joint break force increased significantly, which was due to the increase in the combined area and interface strength. The increase in interfacial strength was due to the decrease in interface defects and gaps. It was worth mentioning that the

Fig. 9 Detailed SEM images of joint welded at 1.75V: (a) left edge region, (b) right edge region, (c) area D and (d) area E
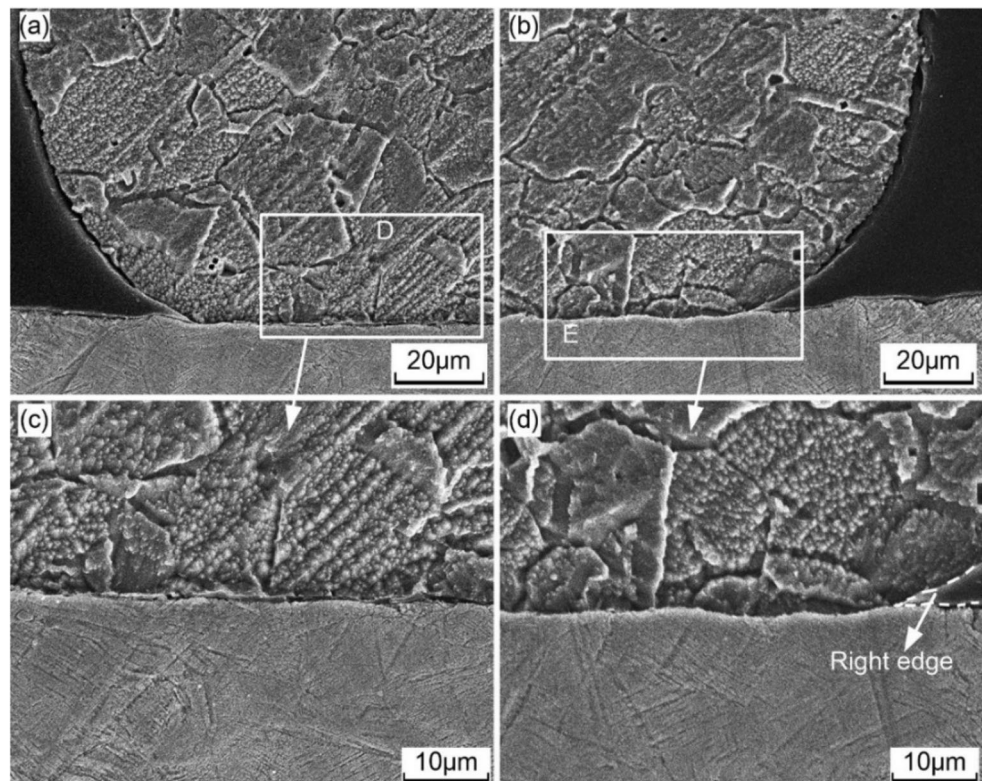

maximum joint breaking force (1.03 N) was achieved at the welding voltage of 2.05 V. When the welding voltage exceeded 2.05 V and continued to increase, since excessive heat was generated and softened Cu wire, the joint breaking force eventually decreased. This phenomenon was confirmed by measuring the Vickers microhardness of the joint (HV 59) welded at the welding voltage of 2.15 V and the as-received wire (HV85). Therefore, the welding process needs sufficient heat to form joints and improve the strength of joints, but excessive heat can degrade the Cu wire. As for the length of the joints, its actual change was not significant.

Figure 11 shows the tensile fracture modes and detailed fracture microstructure of the joints welded at different voltages. It can be seen from the detailed microstructure of the partial pullout fracture that a large number of elongated tearing ribs with different extension directions are distributed on the cross section of the Cu wire. In addition, there are many dimples in some areas, which are typical features of ductile fracture. As the welding voltage increased, the joint failure mode changed from interfacial fracture (1.75 V) to partial

pullout fracture (above 1.85 V), and the position of partial pullout fracture also moved backward, as shown in Fig. 11. The characteristic strength-voltage curve of the joint was due to the combined effect of the expansion of the bonding area, the improvement of interfacial strength, and the amount of heat input (Fig. 3(b)). When the welding voltage was 1.75 V, due to the low heat input, there were still gaps (Fig. 8(a)) and residual carbides (Fig. 11(b)) remained on the faying surface, so the interfacial bonding was weak and the joint fractured at the bonding interface. However, due to the special shape of the electrode, the front-end of the welded joint first contacted the electrode, which made the interfacial bonding of the front part of the joint better than the rear interfacial

Table 2 EDX analysis results of regions A, D, and E in Fig. 8(a), Fig. 9(a), and Fig. 9(b), wt.%

Region	C	Cu	Sn
A	0.000	98.767	1.233
D	0.000	98.690	1.310
E	0.000	98.727	1.273
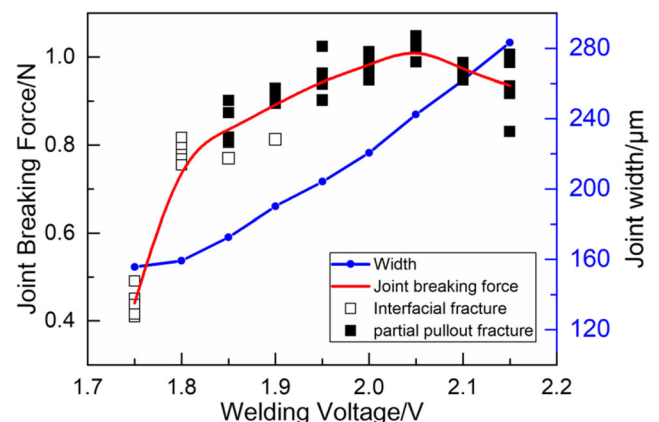
Fig. 10 Effects of welding voltage on breaking force and width of joint

Fig. 11 (**a**, **b**) The interfacial fracture and the C distribution at 1.75 V. (**c**, **d**) The partial pullout fracture and the C distribution at 1.85 V. (**e**, **f**) The partial pullout fracture at 2.05 V and 2.15 V, respectively
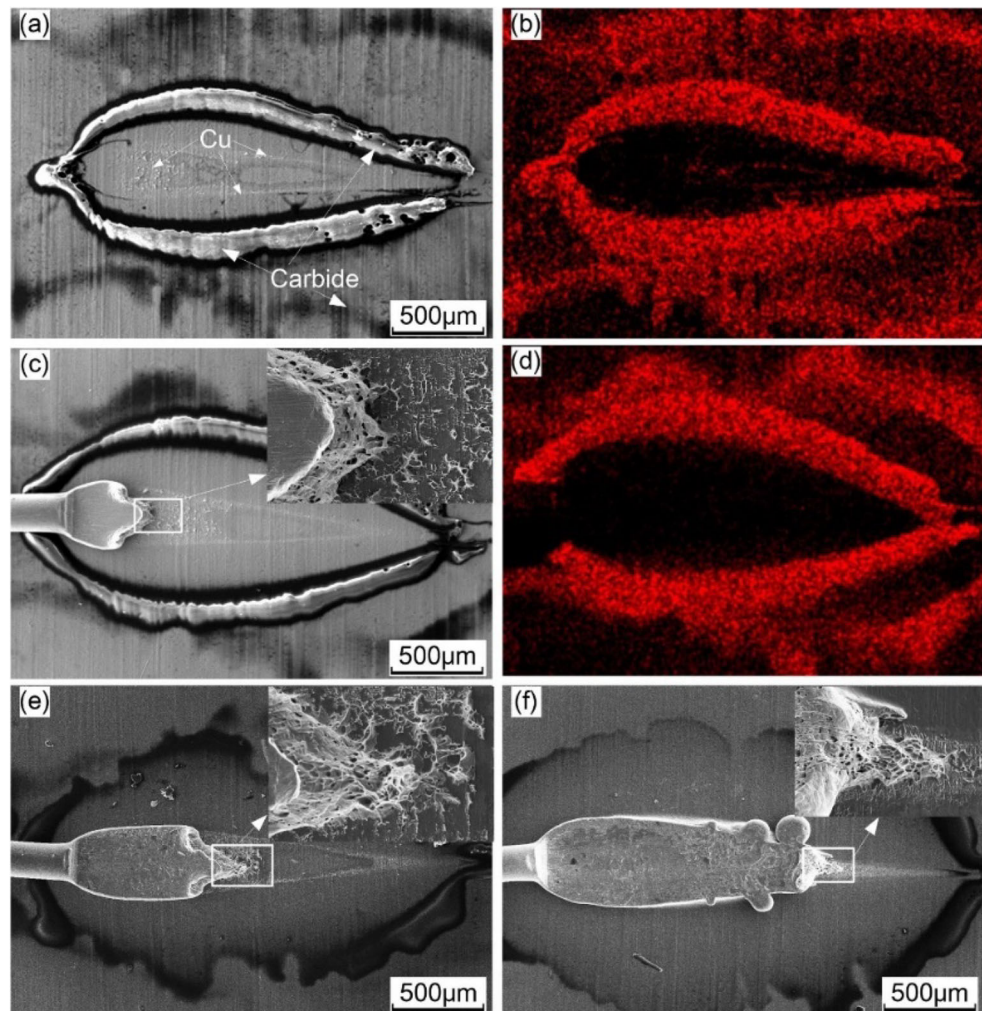
bonding, so there was residual structure Cu wire on the fracture surface (Fig. 11(a)). As the input heat increased, the bonded area (as indicated by the increase of the joint width) and interfacial strength (such as the elimination of residual carbides, as shown in Fig. 11(d)) increased, which improved the joint breaking force. At the same time, as the heat input increase, the strong part of the joint gradually expanded from the front-end to the entire joint, so the fracture position gradually moved back. It was worth noting that when the welding voltage was 2.15 V, the fracture position was located at the end of the joint, which was caused by the softening of the joint end due to excessive input heat.

3.4 Joint formation

In order to form a joint in this RTMW process, heat and pressure were provided in the form of resistance heat and electrode force to eliminate some obstacles (such as surface roughness, oxide layer, or pollution) [20]. At the initial stage, under the action of resistance heating and electrode force, the insulated coating of the Cu wire was expelled from the faying

interface (Fig. 6), providing an opportunity for metal-to-metal bonding. Meanwhile, significant plastic deformation occurred in the Cu wire, and the surface asperities at the faying surface were also eliminated, resulting in the intimate contact of two base metals (Fig. 7 and Fig. 8). In addition, at a temperature of 300–700 °C, the oxide (mainly copper oxides) at the bonding interfaces was thermally decomposed [23] and dissolved into the base metals.

Based on the previous results and discussion, a process sequence of the RTMW process was proposed for the insulated Cu wire and phosphor bronze sheet. First, the insulated copper wire underwent plastic deformation under the influence of squeeze force corresponding to the squeeze time, as shown in Fig. 2 (stage 1). Second, the insulated coating was heated, liquefied, and expelled from the faying surface (stage 2). Subsequently, the Cu wire experienced conspicuous plastic deformation under the effect of Joule heat and electrode force. Finally, a solid-state joint was formed (stage 3). When the welding voltage was further increased, the fusion occurred on the upper surface of two base metals; however, no nugget

Table 3 Scheme and results of the orthogonal experiment

Serial no.	U (V)	T (ms)	F_E (N)	Joint breaking force (N)	Joint length (μm)	Joint width (μm)
a	1.9	16	8	0.2081	1501.26	116.25
b	1.9	18	10	0.3674	1507.91	151.25
c	1.9	20	12	0.8603	1498.42	176.07
d	1.9	22	14	0.7406	1500.98	227.98
e	1.9	24	16	0.5849	1507.30	265.06
f	1.95	16	10	0.3152	1501.26	151.67
g	1.95	18	12	0.8915	1501.38	176.80
h	1.95	20	14	0.7143	1503.51	219.83
i	1.95	22	16	0.5329	1506.62	254.68
j	1.95	24	8	0.7361	1503.93	180.42
k	2.0	16	12	0.9904	1504.37	174.62
l	2.0	18	14	0.7944	1508.11	213.15
m	2.0	20	16	0.6620	1503.93	255.43
n	2.0	22	8	0.8509	1504.37	178.75
o	2.0	24	10	1.1609	1508.11	230.50
p	2.05	16	14	0.8593	1498.17	210.96
q	2.05	18	16	0.5805	1508.82	258.38
r	2.05	20	8	0.8259	1506.07	177.50
s	2.05	22	10	1.0608	1501.35	235.98
t	2.05	24	12	1.0850	1502.93	235.98
u	2.1	16	16	0.6970	1507.72	241.50
v	2.1	18	8	0.6449	1503.27	174.58
w	2.1	20	10	1.0794	1504.15	231.69
x	2.1	22	12	1.0252	1499.14	274.70
y	2.1	24	14	1.0283	1499.56	299.17

was observed at the bonding interface (Fig. 7(e) and Fig. 8(d–f)). Therefore, the formed joint between the insulated Cu wire and phosphor bronze sheet through the RTMW process was a solid-state bonding.

3.5 Design of orthogonal experiment

The bonding strength of insulated copper wire and thin sheets is the focus of the bonding process. According to the previous tests, the bonding process parameters were initially determined to be in the following range: welding voltage (U) was 1.9~2.1 V, welding time (T) was 16~24 ms, and electrode force (F_E) was 8~16 N. The scheme and results of the orthogonal experiment are listed in Table 3. In the orthogonal experiment design, three factors with five levels were tested, i.e. electrode force, welding voltage, and welding time. Range (R) analysis was performed on the obtained data. The analysis results

Table 4 Range analysis of orthogonal test results

|	Joint breaking force			Joint length			Joint width		
	U	T	F_E	U	T	F_E	U	T	F_E
k1	0.5523	0.6140	0.6532	1503.17	1502.56	1503.78	187.32	178.99	165.50
k2	0.6380	0.6557	0.7728	1503.34	1505.90	1504.56	196.67	194.83	200.21
k3	0.8917	0.8284	0.9705	1505.78	1503.22	1501.25	210.49	212.10	213.74
k4	0.8823	0.8421	0.8167	1503.47	1502.49	1502.07	229.87	234.41	234.21
k5	0.8950	0.9190	0.6967	1502.77	1504.37	1502.07	244.32	248.33	255.00
R	0.3427	0.3050	0.3173	3.01	3.41	5.63	57.00	69.34	89.50
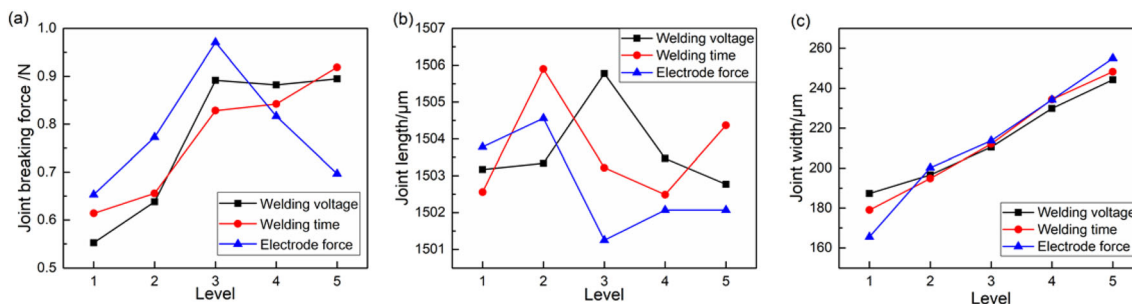
Fig. 12 Effects of three parameters on (**a**) joint breaking force, (**b**) joint length, and (**c**) joint width

are shown in Table 4, and the relationship between each factor and the response is shown in Fig. 12. From Table 4, the optimum process parameters for joint breaking force of insulated Cu wire were obtained as follows: welding voltage was 2.1 V, welding time was 24 ms, and electrode force was 12 N. Under this condition, the average achievable joint breaking force was 1.1723 N, which was about 83.7% of the breaking force of the as-received wire (1.4 N). In contrast, the maximum joint breaking force obtained by the RMW process was approximately 79% of the as-received wire [22].

In order to understand the significance of each factor to the response more intuitively, it is necessary to normalize the range data. Figure 13 shows the normalized contribution of various parameters for different responses.

It can be seen from Table 4 and Fig. 12(a) that the welding voltage is the most important factor affecting the strength of the joint, followed by the electrode force, and the welding time also has a certain effect on the strength of the joints. In addition, the contribution of three parameters to the length of the joints can be sorted from high to low as follows: electrode force > welding time > welding voltage. However, in practice, the change in the joints' length is not significant. It can be speculated that this situation is related to the thickness of the electrode. Finally, for the width of the joint, the electrode force is the most important parameter, the welding time is also relatively significant, and the
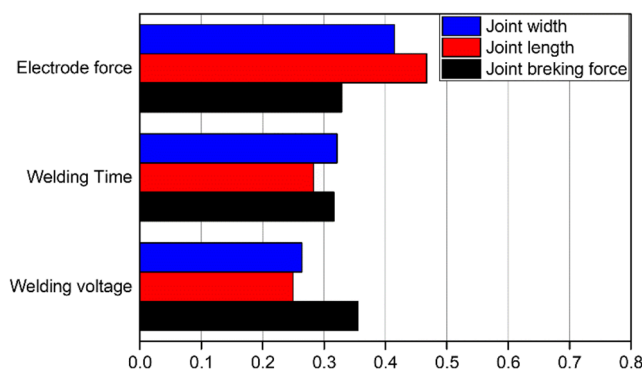
welding voltage has relatively small effect. The above conclusions can be drawn intuitively from Fig. 13.

The above analyses of the influence of various factors on different responses can preliminarily have clarified the relationship between the factors and responses. In order to obtain the joint with good performance, it is necessary to comprehensively analyse the influence of welding parameters on the performance.

4 Conclusion

This study proposed to use the RTMW process to weld insulated copper wire and phosphor bronze sheet, and conducted weldability experiments of the process. The mechanism of RTMW was investigated by detailed mechanical testing and microstructure examinations. The main conclusions are summarized as follows:

1. The RTMW process conducts heat from the bulk resistance of the electrode to the base metals and the generated heat and the electrode force are used to obtain joints. In contrast, the RMW process utilizes the resistance heat generated at the faying surface to weld. Finally, the joints obtained by the RTMW process can meet the industry quality assurance acceptance standard.

2. As the voltage increased, the joint width increased monotonically. However, as the welding voltage increased, the joint breaking force first increased due to increased bonding area and interfacial bonding strength, and then decreased due to softening of copper wire caused by overheating. At a low voltage, the welding joints had an interfacial fracture. At a higher voltage, the bonding area expanded, the interface strength increased, and the amount of heat input increased; thus, the joint fracture mode changes to pullout fracture, and the fracture mechanism is a ductile fracture.

3. The RTMW of insulated Cu wire to phosphor bronze sheet included the following three stages: (1) cold wire deformation; (2) removal of insulated coating; and (3) solid-state bonding. It is worth noting that even at

Fig. 13 The normalized contribution of three parameters for different responses

higher welding voltage, no nugget was observed in the faying surface.

4. Based on the results of the single-factor experiment (voltage), a multi-factor orthogonal experiment was conducted, and the significant order of the influence of each process parameter on the joint breaking force, joint length, and joint width was obtained. For the joint breaking force, the significance of different parameters can be sorted from high to low as follows: welding voltage > electrode force > welding time. For the joint width, the significance of the parameters was in the following order: electrode force > welding time > welding voltage. The length of the joint was mainly limited by the thickness of the electrode.

5. The optimal process parameters for the joint breaking force were obtained as follows: welding voltage was 2.1 V, welding time was 24 ms, and electrode force was 12 N. Under this condition, the average achievable of the joint breaking force was 1.1723 N, which was about 83.7% of the breaking force of the as-received wire (1.4 N).

Code availability   Not applicable

Authors' contributions   Zhiyuan Cui: investigation, writing—original draft. Yuanbo Li: conceptualization, resources. Lingyu Chen: supervision. Songjie Wen: validation. Songming Guo: investigation.

Declarations

Conflict of interest   The authors declare no competing interests.

References

1. Gan CL, Hashim U (2015) Evolutions of bonding wires used in semiconductor electronics: perspective over 25 years. J Mater Sci-Mater Electron 26(7):4412–4424. https://doi.org/10.1007/s10854-015-2892-8

2. Makhloufi A, Aoues Y, El Hami A (2016) Reliability based design optimization of wire bonding in power microelectronic devices. Microsyst Technol-Micro-Nanosyst-Inf Storage Process Syst 22(12):2737–2748. https://doi.org/10.1007/s00542-016-3151-5

3. Tada N, Tanaka T, Uemori T, Nakata T (2017) Evaluation of Thin Copper Wire and Lead-Free Solder Joint Strength by Pullout Tests and Wire Surface Observation. Crystals 7(8):10. https://doi.org/10.3390/cryst7080255

4. Chauhan P, Zhong ZW, Pecht M (2013) Copper Wire Bonding Concerns and Best Practices. J Elec Mater 42(8):2415–2434. https://doi.org/10.1007/s11664-013-2576-1

5. Hollatz S, Heinen P, Limpert E, Olowinsky A, Gillner A (2020) Overlap joining of aluminium and copper using laser micro welding with spatial power modulation. Weld World 64(3):513–522. https://doi.org/10.1007/s40194-020-00848-9

6. Liu PS, Tong LY, Wang JL, Shi L, Tang H (2012) Challenges and developments of copper wire bonding technology. Microelectron Reliab 52(6):1092–1098. https://doi.org/10.1016/j.microrel.2011.12.013

7. Xu H, Liu C, Silberschmidt VV, Chen Z, Acoff VL (2011) Effect of ultrasonic energy on nanoscale interfacial structure in copper wire bonding on aluminium pads. J Phys D-Appl Phys 44(14):5. https://doi.org/10.1088/0022-3727/44/14/145301

8. Murali S, Srikanth N, Wong YM, Vath CJ (2007) Fundamentals of thermo-sonic copper wire bonding in microelectronics packaging. J Mater Sci 42(2):615–623. https://doi.org/10.1007/s10853-006-1148-7

9. Zhong ZW (2011) Overview of wire bonding using copper wire or insulated wire. Microelectron Reliab 51(1):4–12. https://doi.org/10.1016/j.microrel.2010.06.003

10. Leong HY, Yap BK, Khan N, Ibrahim MR, Tan LC, Faiz M (2014) Stitch bond strength study in insulated Cu wire bonding. Mater Res Innov 18:264–268. https://doi.org/10.1179/1432891714z.0000000001018

11. Murali S, Sureshkumar V, Wan LM, Wei TC, Xi Z, Ieee (2015) Interfacial Reaction and Thermal Ageing of Ball and Stitch Bonds. Paper presented at the 2015 Ieee 17th Electronics Packaging and Technology Conference (Eptc),

12. Kumar JP (2020) Effect of process parameter characteristics on joint strength during ultrasonic metal welding of electrical contacts. Weld World 64(1):73–82. https://doi.org/10.1007/s40194-019-00820-2

13. Tian Y, Wang C, Lum I, Mayer M, Jung JP, Zhou Y (2008) Investigation of ultrasonic copper wire wedge bonding on Au/Ni plated Cu substrates at ambient temperature. J Mater Process Technol 208(1-3):179–186. https://doi.org/10.1016/j.jmatprotec.2007.12.134

14. Shi WQ, Huang J, Xie YP, Li YQ, An FJ (2017) Laser micro-welding technology for Cu-Al dissimilar metals and mechanisms of weld defect formation. Int J Adv Manuf Technol 93(9-12):4197–4201. https://doi.org/10.1007/s00170-017-0814-z

15. Singh G, Haseeb A (2019) Influence of laser power on bonding strength for low purity copper wire bonding technology. Microelectron Eng 211:1–4. https://doi.org/10.1016/j.mee.2019.03.018

16. Tabatabaei HM, Nishihara T (2017) Friction stir forming for mechanical interlocking of insulated copper wire and Zn-22Al superplastic alloy. Weld World 61(1):47–55. https://doi.org/10.1007/s40194-016-0406-9

17. Cong S, Zhang WW, Wang YS, Wen ZJ, Tian YH (2018) Effect of heat input on failure mode and connection mechanism of parallel micro-gap resistance welding for copper wire. Int J Adv Manuf Technol 96(1-4):299–306. https://doi.org/10.1007/s00170-018-1596-7

18. Zhang WW, Cong S, Wen ZJ, Liu Y, Wang YS, Tian YH (2017) Experiments and reliability research on bonding process of micron copper wire and nanometer gold layer. Int J Adv Manuf Technol 92(9-12):4073–4080. https://doi.org/10.1007/s00170-017-0490-z

19. Chen F, Wang YS, Sun SD, Ma ZW, Huang X (2019) Multi-objective optimization of mechanical quality and stability during micro resistance spot welding. Int J Adv Manuf Technol 101(5-8):1903–1913. https://doi.org/10.1007/s00170-018-3055-x

20. Fukumoto S, Zhou Y (2004) Mechanism of resistance microwelding of crossed fine nickel wires. Metall Mater Trans A-Phys Metall Mater Sci 35A(10):3165–3176. https://doi.org/10.1007/s11661-004-0061-4

21. Liu Y, Tian YH, Liu BL, Xu JK, Feng JY Wang CX Interconnection of Cu wire/Au plating pads using parallel gap resistance microwelding process. In: 17th International Conference

on Electronic Packaging Technology (Icept), Wuhan, CHINA, Aug 16-19 2016. IEEE. USA, NEW YORK, pp 43–46. https://doi.org/10.1109/ICEPT.2016.7583086

22. Mo B, Guo Z, Li Y, Huang Z, Wang G (2011) Mechanism of Resistance Microwelding of Insulated Copper Wire to Phosphor Bronze Sheet. Mater Trans 52(6):1252–1258. https://doi.org/10.2320/matertrans.M2011013

23. Messler RW Jr (1999) Principles of Welding: Processes, Physics, Chemistry. In: and Metallurgy. Wiley, New York. https://doi.org/10.1002/9783527617487